Title:

Radar-derived Properties of the InSight Landing Site in Western Elysium Planitia on Mars

Authors:

Nathaniel E. Putzig [1,2]

Gareth A. Morgan [3]

Bruce A. Campbell [3]

Cyril Grima [4]

Isaac B. Smith [1,2]

Roger J. Phillips [5,6]

Matthew P. Golombek [7]

[1] Department of Space Studies, Southwest Research Institute, Boulder, CO 80302

[2] Now at: Planetary Science Institute, Lakewood, CO 80401

[3] Center for Earth and Planetary Studies, Smithsonian Institution, Washington, DC, 20560

[4] Institute for Geophysics, University of Texas, Austin, TX 78758

[5] Planetary Science Directorate, Southwest Research Institute, Boulder, CO 80302

[6] McDonnell Center for the Space Sciences and Department of Earth and Planetary Sciences, Washington University, St. Louis, MO 63130

[7] Jet Propulsion Laboratory, California Institute of Technology, Pasadena, CA 91109

Abstract

We carried out an assessment of surface and subsurface properties based on radar observations of the region in western Elysium Planitia selected as the landing site for the InSight mission. Using observations from Arecibo Observatory and from the Mars Reconnaissance Orbiter's Shallow Radar (SHARAD), we examined the near-surface properties of the landing site, including characterization of reflectivity, near-surface roughness, and layering. In the Arecibo data (12.6-cm wavelength), we found a radar-reflective surface with no unusual properties that would cause problems for the InSight radar altimeter (7-cm wavelength). In

addition, the moderately low backscatter strength is indicative of a relatively smooth surface at ~10-cm scales that is composed of load-bearing materials and should not present a hazard for landing safety. For roughness at 10–100 m scales derived from SHARAD data, we find relatively low values in a narrow distribution, similar to those found at the Phoenix and Opportunity landing sites. The power of returns at InSight is similar to that at Phoenix and thus suggestive of near-surface layering, consistent with a layer of regolith over bedrock (e.g., lava flows) that is largely too shallow (<10–20 m) for SHARAD to discern distinct reflectors. However, an isolated area outside of the ellipse chosen in 2015 for InSight's landing shows faint returns that may represent such a contact at depths of ~20–43 m.

Introduction

As part of a broader effort to select the landing site for the InSight spacecraft (Golombek et al., this issue), we assessed reflectivity, near-surface roughness, and layering in the landing-site region using two radar data sets, each of which offers unique constraints for landing-site safety considerations and instrument operations. Of primary interest was the assessment from the radar data as to whether the surfaces at the sites under consideration are (1) of high enough reflectivity to ensure the descent radar altimeter would function properly, (2) composed of sufficiently competent materials to bear the load of the spacecraft, and (3) smooth enough to be relatively free of hazardous slopes and large rocks at the radar-wavelength scales. The latter consideration has bearing on deployment of instruments — specifically, a seismometer and a heat-flow probe — and on the broader goals of the InSight mission, which aims to determine the size and state of the Martian core, mantle, and crust as part of an effort to better understand the differentiation of terrestrial planets (Banerdt et al., 2013).

Arecibo Observatory's S-band radar (Harmon et al., 1999; 2012) provides information on the near-surface reflectivity, dielectric, and roughness properties, relative to its 12.6-cm wavelength, for the entire InSight landing area. The radar images have a best lateral resolution of ~3 km at the Martian surface, but the echoes are sensitive to small-scale surface roughness and to rocks larger than a few cm within the signal's penetration depth (1–3 m). Arecibo image data provide critical information on the surface reflectivity at a wavelength similar to the C-band (7-cm) descent radar

altimeter and velocimeter on InSight used to initiate powered descent, measure the closing velocity, and throttle the descent engines to ensure a soft landing (Golombek et al., this issue). In addition, the surface roughness can be constrained by comparison with well-calibrated observations of terrestrial-analog surfaces (e.g., Campbell, 2001; 2009; 2012). Low-power returns may also indicate a fine-grained mantling material, which can be investigated by other means (e.g., orbital radar, thermal spectroscopy). Such observations have great significance to assessment of InSight landing safety and the potential for successful deployment of the thermal probe that is designed to hammer itself up to 5 m depth beneath the surface.

The Shallow Radar (SHARAD) on the Mars Reconnaissance Orbiter (MRO) is best known for its use in mapping the internal structures of polar deposits (Phillips et al., 2008; 2011; Putzig et al., 2009; Holt et al., 2010; Smith and Holt., 2010; Brothers et al., 2015; Smith et al., 2016), establishing the ice-rich nature of lobate debris aprons (Holt et al., 2008; Plaut et al., 2009), and assessing the nature of volcanic deposits (Campbell et al., 2008a; Carter et al., 2009a; 2009b; Morgan et al., 2013; 2015). The latter include materials located a few 100 km east of the InSight landing area (Morgan et al., 2013; 2015). SHARAD penetration depths for low-latitude targets range from tens of meters in basaltic flow units (Morgan et al., 2015) to several hundred meters within the Medusae Fossae Formation (Carter et al., 2009b). SHARAD also offers a view of surface roughness in terms of root-mean-squared (RMS) slope on horizontal scales of 10–100 m and in footprints of 3–4 km, depending on local topographic variability (Campbell et al., 2013). Alternatively, one may employ a model-based statistical analysis to SHARAD returns to estimate material properties and roughness in terms of RMS heights (Grima et al., 2014). These techniques complement smaller-scale roughness information from Arecibo data and extrapolated slopes and pulse-width measurements from Mars Orbiter Laser Altimeter (MOLA) (Anderson et al., 2003; Neumann et al., 2003) as well as the larger-scale roughness estimate from MOLA altimetry (Kreslavsky and Head, 2000).

Past landing sites have been targeted extensively with SHARAD, yielding roughness estimates consistent with landed observations and other data (Putzig et al., 2014). Subsurface detections at landing sites have thus far been confined to the ‘Green Valley’ of the Phoenix site, with returns from ~25 m depth mapped over 2900 km^2 that may represent the base of ground ice

(Putzig et al., 2014). An important element of these studies is the use of techniques to distinguish subsurface features from off-nadir surface features or surface sidelobes (Holt et al., 2006; Choudhary et al., 2016). In the region around the InSight landing site, SHARAD coverage density is relatively low due to restrictions imposed by the provision of MRO communications support to the Curiosity rover, which is located a few 100 km to the south.

In this paper, we describe the data sets and our analysis methods and we discuss our results in terms of their impact on landing-site safety and their relationship to observations at previous landing sites.

Methods

The focus of this study was to assess radar reflectivity, radar-inferred roughness, and near-surface density and to search for evidence of subsurface interfaces in the region of the proposed InSight landing area with data from Arecibo and SHARAD. A primary concern with regard to selection of the InSight landing site was ensuring that the reflectivity of the surface, a measure related to its bulk density (e.g., see Golombek et al., 1997), is not so low as to risk landing on a surface that cannot support the load of the spacecraft, as may be the case for so-called stealth regions of extremely low reflectivity (Muhleman et al., 1991).

We used an Arecibo 12.6-cm radar image obtained in October 2005 (Harmon et al., 2012) to estimate the maximum surface roughness or rock abundance at scales comparable to the radar wavelength (Campbell, 2001; 2009). In particular, we used the same-sense circular (SC) polarization echoes, which are most strongly modulated by the small-scale roughness and rock abundance of the surface and shallow subsurface. Power in the image was scaled to a common incidence angle of 30° using a cosine function. We also studied patterns of the radar echoes relative to the geology of the target region to assess possible changes in surface density or mantling cover, a routine practice in lunar radar studies (e.g., Campbell et al., 2008b).

With SHARAD data, we followed the method of Campbell et al. (2013) in computing a roughness parameter from the ratio of echo power integrated over a range of incidence angles to the peak echo power. This measure of roughness is independent of surface reflectivity and is related to the RMS slope of the surface at scales of 10 to 100 m. We limited the integration to the

first 20 vertical samples (0.713 μs) below the surface, corresponding to incidence angles < 1.5° and depths < ~60 m, to avoid the inclusion of most shallow subsurface returns (i.e., any at greater depths). We then mapped results for the available SHARAD coverage in the region and compared values for the proposed InSight landing ellipses with those for surrounding terrains and for past landing sites.

Radar statistical reconnaissance (RSR) (Grima et al. 2012; 2014) presents an alternative and complementary approach to assessing surface properties from SHARAD data. This method separates the radar data into coherent and incoherent components by fitting the peak-echo amplitude distribution with a probability density function. One may then extract dielectric permittivity and RMS height using a backscattering model applicable over some range of conditions (e.g., the small-perturbation model, SPM, or the integral-equation method, IEM). To obtain quantitative estimates of dielectric permittivity and RMS height from the radar data, one must choose a calibration zone wherein the permittivity is reasonably well-known. For this study, we chose a relatively smooth region of the south polar layered deposits (SPLD) where it is reasonable to assume properties consistent with water ice, e.g., a dielectric permittivity of 3.1.

In addition, for each orbital pass over the InSight region with SHARAD observations, we produced radargrams, along-track profiles showing the returned power vs. delay time in an image format. We searched for potential subsurface reflections—returns delayed relative to the nadir surface returns in the radargrams—using simulations and custom processing as needed to identify and suppress off-nadir returns and sidelobes while enhancing subsurface returns (e.g., Holt et al., 2008; Putzig et al., 2014). Where potential subsurface interfaces were found, we mapped their extent and provided an interpretation of the subsurface material properties.

Results

The Arecibo SC-polarization image at 12.6-cm wavelength (Fig. 1) shows a radar-reflective surface with no indications of anomalous properties in and around the InSight region and thus one that should be radar reflective for the C-band (7-cm) altimeter on InSight. The backscatter strength from the final four sites in the InSight region is moderately low (averaging -17.0 to -16.2 dB, with -16.4 dB in the final ellipse). Being in the middle of the typical diffuse reflectivity

range, these sites are not solely comprised of rock-poor, porous material at the 12.5-cm scale. The InSight ellipses are brighter than a large lobe of the Medusae Fossae Formation (-18.9 dB) several hundred km to the east in the same image, a difference that is more pronounced when considering incidence-angle effects. At the same time, the InSight ellipses are notably darker than returns in the same image from volcanic flows of the Elysium Rise (-14.3 dB) to the north and of Elysium Planitia (-8.4 dB) to the east. The values in the InSight region are similar to those of a field site on Kilauea with a moderately rocky surface (Campbell, 2001), slightly higher than those of Viking Lander 1 (-17 dB at 36°), and considerably higher than those of Viking Lander 2 (-19 dB at 47°). Thus, surface rock abundance in the 2–10 cm range at InSight is likely to range from slightly to significantly higher than at the two Viking sites. Unfortunately, the InSight region was too close to the sub-radar point (at about 23° incidence) to obtain useful values for the circular-polarization ratio.

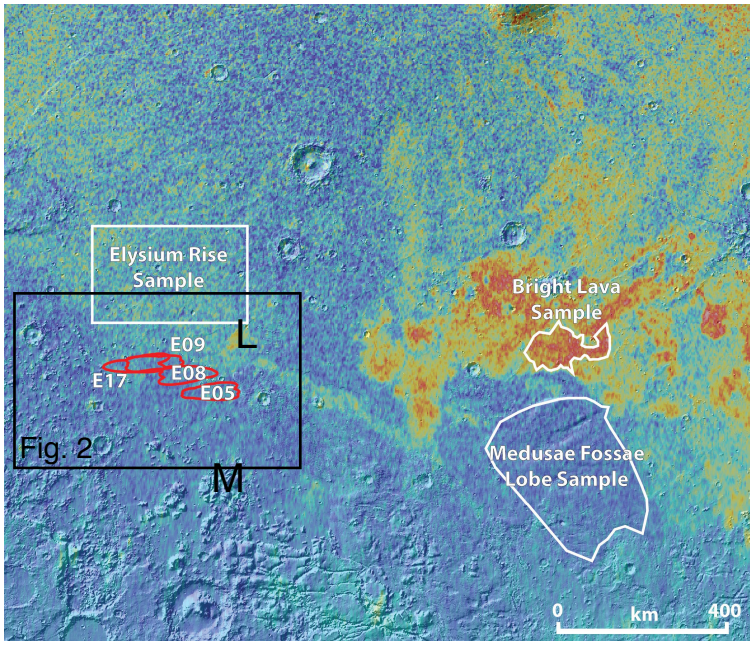

Figure 1. Arecibo SC-polarization image showing power (higher for brighter colors) at 12.6-cm wavelength. Sample regions, including InSight landing ellipses, indicate areas used for values reported in text. L and M symbols indicate lava and mesa locations used for SHARAD RMS-height roughness analysis (see Fig. 5).

The InSight spacecraft will employ a 7-cm-wavelength radar altimeter during decent. A major concern of landing safety is the establishment of surfaces that are suitably reflective within the landing ellipses to enable accurate measurements of the spacecraft's altitude. The Arecibo measurements demonstrate that there are no surfaces with anomalously low backscatter (which would compromise the onboard range measurements) within any of the ellipses.

Our map of SHARAD-derived RMS-slope roughness parameter (Fig. 2) indicates that the final four sites are a part of the region that is smoothest at 10–100 m scales, except for the lava flows just to the northeast that are somewhat smoother. We see a similarity of the SHARAD-derived roughness map (Fig. 2) to the MOLA pulse-spread and 100-m extrapolated roughness maps (Figs. 19 and 20 of Golombek et al., this issue), suggesting both instruments are measuring a smooth surface at this length scale.

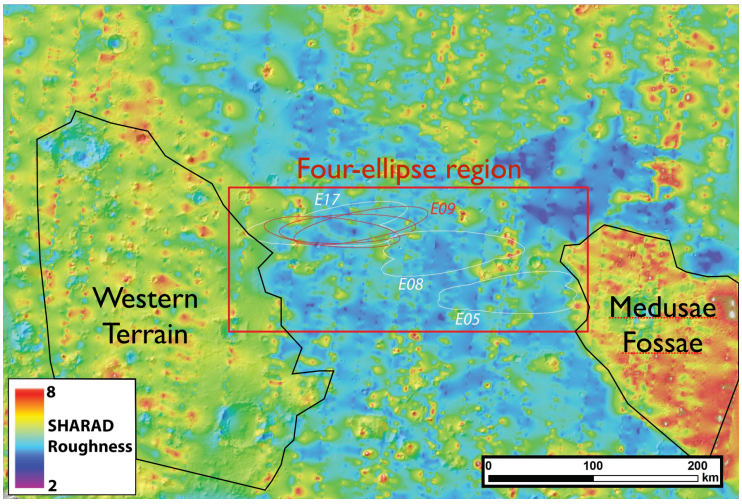

Figure 2. Map of SHARAD-derived RMS-slope roughness parameter in the InSight region. Areas used to assess roughness distributions indicated by black, red, and white polygons (see Fig. 3).

These sites are both smoother and have a narrower distribution of roughness relative to the nearby areas to the east and west (Fig. 3a). There are only minor differences in the roughness

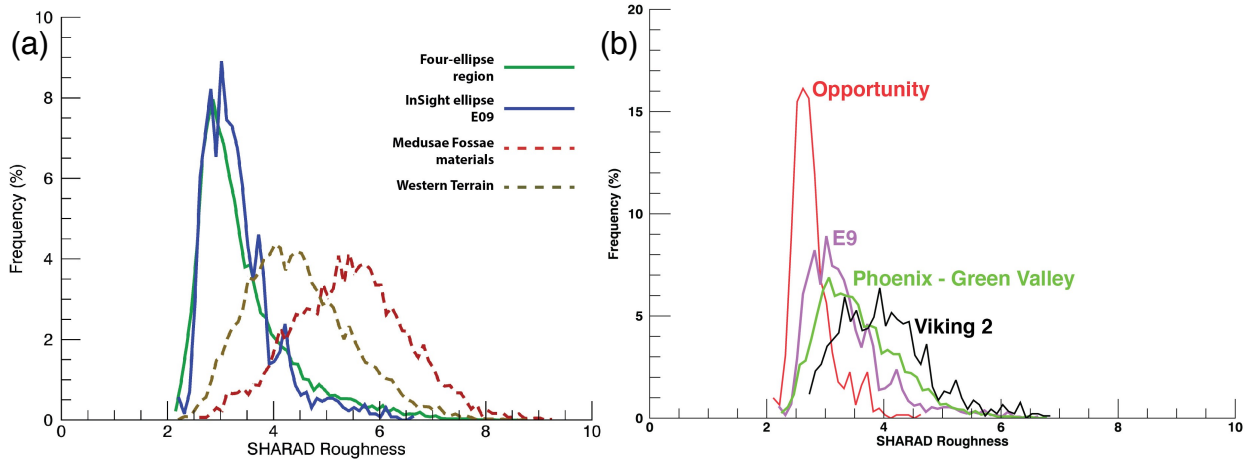

Figure 3. (a). Distributions of SHARAD RMS-slope roughness parameter in the final four landing ellipses (green), in the selected ellipse E09 (blue), and in rougher terrains to the east (brown) and west (red) See Fig. 2 for locations. (b). Distributions of SHARAD RMS-slope roughness parameter at three earlier landing sites and in ellipse E09 (purple) curve, which is similar to that found in the region surrounding the Phoenix site.

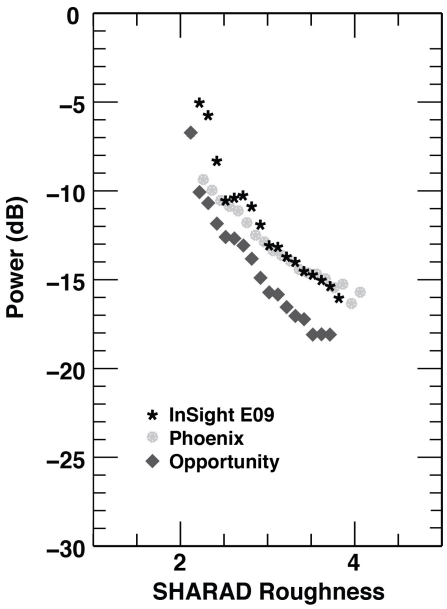

Figure 4. SHARAD roughness parameter vs. power of surface returns for the InSight final ellipse E09 (stars), and the Phoenix landing site (circles), and the MER Opportunity site (diamonds). While roughness distributions are similar for all three sites, the surface-return power is higher for both Phoenix and InSight.

distributions between the final four sites. In comparison to other landing sites, the InSight landing area has a similar distribution of roughness to that of the Phoenix and Meridiani landing sites (Fig. 3b). One distinguishing feature is that the power of the nadir surface returns for a range of values of the roughness parameter at InSight is similar to that of Phoenix but larger by several dB than that of Meridiani (Fig. 4). The Phoenix site is though to have a shallow ice layer extending between a few decimeters to ~35 m depth (Putzig et al., 2014), with large dielectric contrasts at top and bottom presumably contributing to the power of the surface return. In contrast, Meridiani has a stack of sediments up to a few hundred meters thick with no evidence in SHARAD data for large dielectric contrasts (Putzig et al., 2014). Considering that the InSight landing site is within volcanic terrain (i.e., dense lava flows with high permittivity) and extremely unlikely to host ground ice due to the low latitude, the similarity in power is likely explained by the presence of a low density material (e.g., regolith) overlying more intact rock within the upper range cell of the surface return (i.e., within 10–20 m depth), an interpretation also supported by analysis of rocky ejecta craters and fragmentation theory (Golombek et al., this issue).

A preliminary application of the RSR approach to Mars radar echoes provides another means of assessing surface properties in the InSight region (Fig. 5). We followed the methodology of Grima et al. (2014) to assess the fundamental signal components (reflectance and scattering) comprising the histogram of surface echo amplitudes from the E09 ellipses. The small-perturbation model for radar scattering from smoother surfaces yielded an estimated dielectric permittivity for the Elysium Rise lava flows (just to the northeast of the final four sites) of 4.9

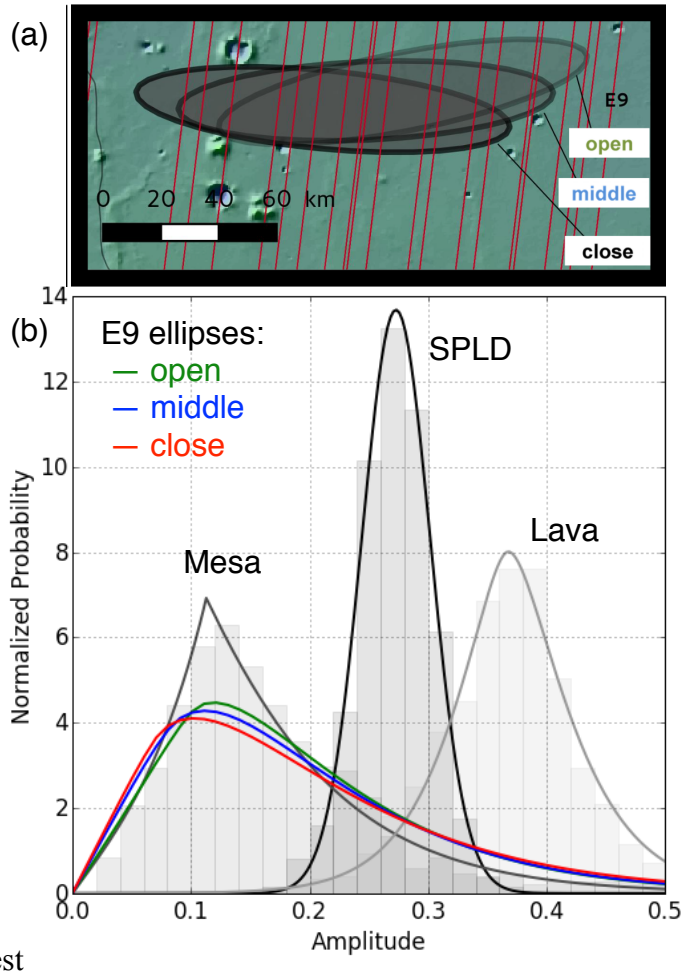

Figure 5. (a) Map of ground tracks crossing the final InSight landing site, showing ellipses for open, middle, and close of launch window. (b) Probability distributions of SHARAD surface-return amplitudes for ellipses (colors), the calibration site in the south polar layered deposits (black), lava flows in the Elysium Rise to the north (light grey), and mesas to the south (dark grey) of the InSight region. See Fig. 1 for lava and mesa locations.

and RMS height of 0.28 m. For the Elysium Planitia flows several hundred km to the east, the same model yielded a dielectric permittivity of 14.0 and RMS height of 0.45 m. These results might suggest a significant degree of variability in surface density between these two sites, although the upper estimate of 14.0 exceeds plausible values of lava flows and may point to a poor match between the SPM and the scattering behavior of the surfaces. In the same vein, the coherent-to-incoherent power ratio is less than unity within the InSight landing ellipses and in some of the nearby rougher terrain (e.g., mesa area in Fig. 5), making their echo statistics incompatible with the SPM. On a qualitative basis, the open, middle, and close variants of the final landing ellipse all have similar statistics, with a slight decrease in coherent power and its ratio to incoherent power (both changes indicative of increasing roughness) as the ellipse rotates clockwise with time of launch. The close ellipse has a slightly broader distribution of amplitudes, indicating more variable terrain. This observation is consistent with the close ellipse including more large craters than the open and middle ellipses (Golombek et al., this issue).

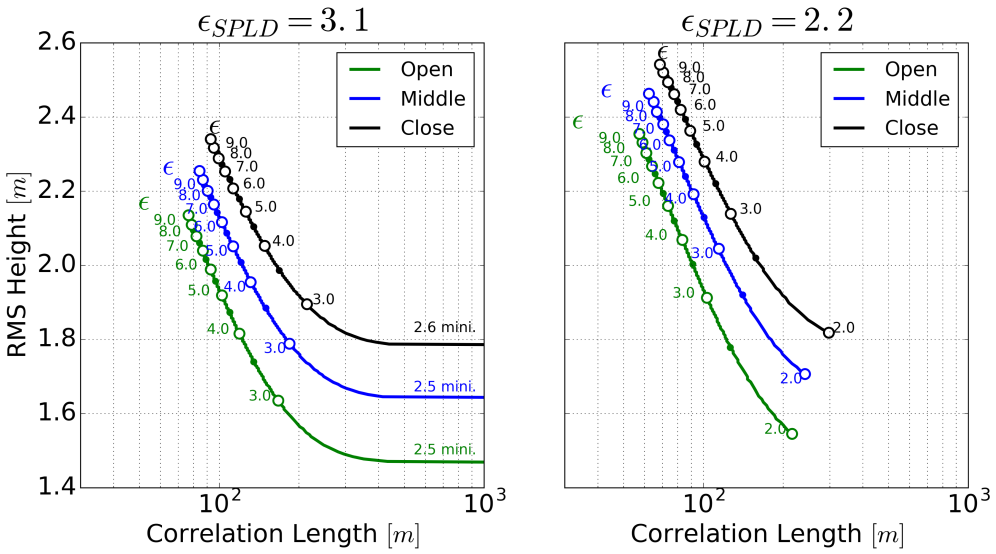

Figure 6. RMS Height as a function of correlation length for the InSight open, middle, and close E09 ellipses. Separate plots show results using different assumed values for the dielectric permittivity calibration region in the south polar layered deposits. Labeled symbols show values using different assumed values for the dielectric permittivity of the surface in the ellipses.

Using the integral equation model (IEM) (Fung et al., 1992), we identified the field of surface properties that are solutions of the previously derived signal components within the E09 ellipses. The IEM is valid for RMS heights up to 20–30% of the radar wavelength (~3–5 m). We assumed a two-layer model (semi-infinite ground overlain by atmosphere), no volume scattering, no multiple scattering, and no shadowing effects (the last two being common at normal incidence). Fig. 6 shows the field of solutions for the surface permittivity, RMS height, and correlation length for the E09 ellipses at the radar horizontal scales. For the SPLD calibration zone, we considered reference dielectric permittivities of 3.1 and 2.2 (Fig. 6). The first value allows up to 3% dust in ice with no porosity and up to 20% dust in ice with 20% porosity, while the later is more appropriate for porous ice (snow) or light dust. Whatever the considered reference permittivity, we can roughly constrain the RMS heights to ~1.5–2.6 m in the E09 ellipses, increasing with permittivity and time of launch, as with the SPM. The effective slope, i.e. the ratio of RMS height with correlation length (Shepard et al., 2001), is approximately the same for a given permittivity. It varies from 0.006 (0.3°) for low permittivities to 0.04 (2.3°) for permittivities up to 9, with the latter a more realistic assumption for the InSight region.

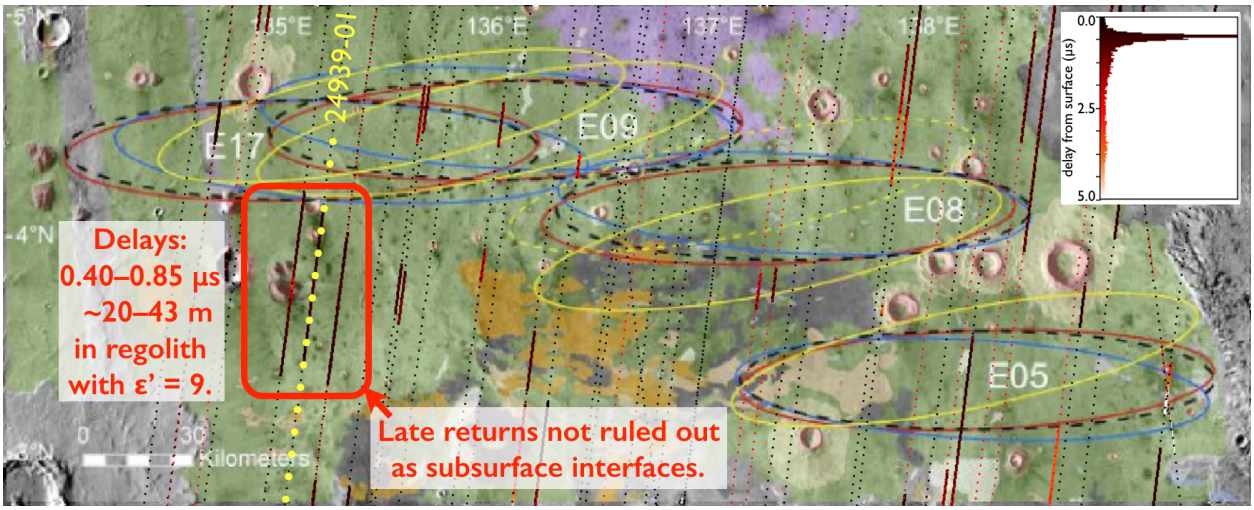

Figure 7. Map of delay times (shades of red) for possible subsurface returns along SHARAD ground tracks (black and red dotted lines). Base is a THEMIS VIS mosaic overlain with terrain map of Golombek et al. (2014). Dotted yellow line indicates track for example from SHARAD observation 24939-01 shown in Fig. 8.

Upon searching through all SHARAD radargrams crossing the InSight region, we identified possible subsurface returns in many locations (Fig. 7). In each case, we produced a corresponding synthetic radargram from a MOLA digital elevation model (DEM). In most instances, we found that the late returns identified as possible subsurface returns correspond to off-nadir surface returns (clutter) seen in the synthetic radargrams. Within the ellipses for the final four sites, we interpret all late returns as surface clutter based on the comparison of SHARAD and synthetic radargrams. However, on four adjacent radargrams, there is a set of low-power, late returns extending ~50 km southward from the southwestern edge of the final ellipse that do not have corresponding features in the synthetics (e.g., Fig. 8). These returns are delayed 0.40–0.85 μs relative to the surface return, corresponding to depths of ~20–43 m in material with a dielectric permittivity of 9 (typical of dense basalt). In an effort to ensure that the possible subsurface returns here are not the result of surface clutter from features not captured in the MOLA DEM, we created additional synthetic radargrams using a DEM produced from High Resolution Stereo Camera (HRSC) images (Klaus Gwinner, pers. comm., and included in Golombek et al., this issue). The DEM is of lower quality in this area and the resulting synthetic appears rather noisy, but there are not indications of a clutter signal corresponding to the weak

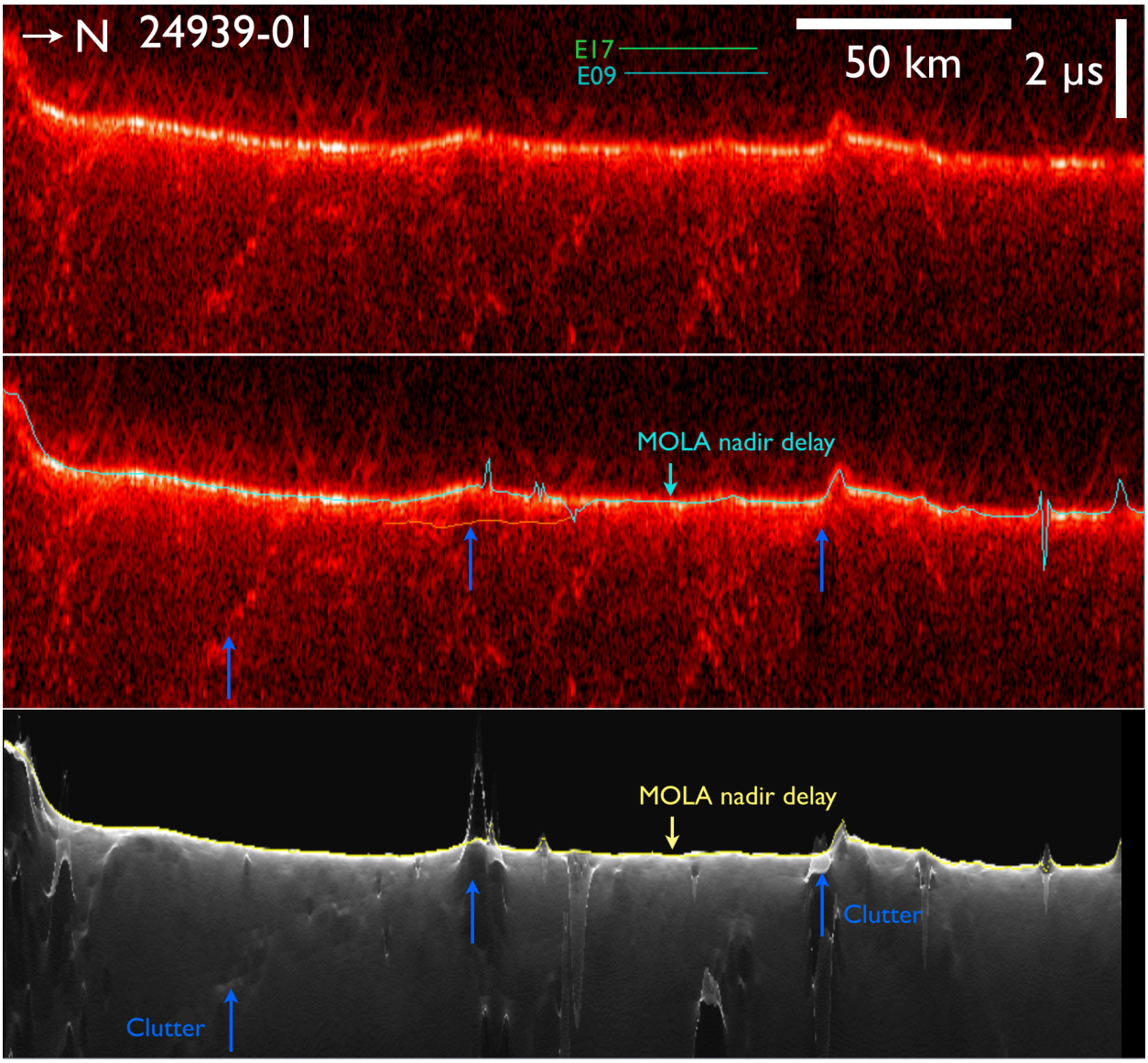

Figure 8. SHARAD radargram (top two panels) showing profiles of power (shades of red) along track vs. delay time. In the middle panel, possible subsurface return is marked with an orange line, and blue arrows indicate late returns for comparison to a synthetic radargram produced from a MOLA DEM (bottom panel). Late returns that appear in the synthetic and labeled “Clutter” are due to off-nadir surface features. Extent of ellipses crossed is shown at top with green and blue lines. See Fig. 7 for ground-track location.

returns seen in the SHARAD radargrams. We interpret these late returns as coming from an interface with a relatively abrupt density contrast, perhaps a contact between regolith and bedrock. It is not clear why the returns are limited to this particular region.

Conclusions

Radar observations provide a unique measure of surface properties that complements those provided by imagery, spectroscopic data, and laser altimetry. Our assessments of radar reflectivity, radar-derived roughness, and near-surface layering in the InSight landing-site region contributed to the certification of the final landing ellipse. In particular, we found that the surfaces at all of the final four sites are (1) sufficiently reflective in Arecibo radar observations to give confidence that the descent radar altimeter will function as intended, (2) composed of materials that are strong enough to support the weight of the spacecraft, and (3) smooth enough to be relatively free of hazardous slopes and large rocks at the radar-wavelength scales. While Arecibo backscatter strengths indicate InSight rock abundance as high or higher than that of the Viking Lander sites, this result pertains to smaller rocks in the 2–10 cm range. No subsurface interfaces have been detected within the final four landing ellipses, but both the power of surface returns and an isolated set of faint returns outside of the final ellipse are suggestive of a shallow (<20 to 43 m depth) layering that may be a boundary between regolith and underlying bedrock.

Acknowledgments

We are grateful to all of the people and organizations who have helped facilitate this work, including the SHARAD Instrument Team, the Italian Space Agency, the MRO Project, and SeisWare International. We thank John Harmon for providing the Arecibo radar data, Klaus Gwinner for providing the HRSC digital elevation model, and two anonymous reviewers for helping us improve the manuscript. Research described in this paper was partially done by the InSight Project, Jet Propulsion Laboratory, California Institute of Technology, under a contract with the National Aeronautics and Space Administration.

References

Anderson, F.S., A.F.C. Haldemann, N.T. Bridges, M.P. Golombek, T.J. Parker, G. Neumann, 2003. Analysis of MOLA data for the Mars Exploration Rover landing sites. J. Geophys. Res. 108, 8084, doi:10.1029/2003JE002125.

Banerdt, W. B., S. Smrekar, K. Huyst, P. Lognonné, T. Spohn, S. Asmar, D. Banfield, L. Boschi, U. Christensen, V. Dehant, W. Folkner, D. Giardini, W. Goetz, M. Golombek, M. Grott, T. Hudson, C. Johnson, G. Kargl, N. Kobayashi, J. Maki, D. Mimoun, A. Mocquet, P. Morgan, M. Panning, W. T. Pike, J. Tromp, T. van Zoest, R. Weber, M. Wieczorek, and T. I. Team (2013), InSight: a Discovery mission to explore the interior of Mars, Lunar Planet. Sci., XLIV., Abstract #1915.

Brothers, T. C., Holt, J. W., and Spiga, A. (2015), Planum Boreum basal unit topography, Mars: irregularities and insights from SHARAD, J. Geophys. Res., 1201357-1375, doi: 10.1002/2015JE004830.

Campbell, B.A., 2001. Radar backscatter from Mars: Properties of rock-strewn surfaces. Icarus 150, 38–47.

Campbell, B.A., 2009. Scale-dependent surface roughness behavior and its impact on empirical models for radar backscatter. IEEE Geosci. Rem. Sensing 47, 3480–3488, doi:TGRS. 2009.2022752.

Campbell, B.A., 2012. High circular polarization ratios in radar scattering from geologic targets. J. Geophys. Res. 117, E06008, doi:10.1029/2012JE004061.

Campbell, B., Carter, L., Phillips, R., Plaut, J., Putzig, N., Safaeinili, A., Seu, R., Biccari, D., Egan, A., and Orosei, R., 2008a. SHARAD radar sounding of the Vastitas Borealis Formation in Amazonis Planitia. J. Geophys. Res. 113, E12010, doi: 10.1029/2008JE003177, 10 p.

Campbell, B.A., Carter, L.M., Hawke, B.R., Campbell, D.B., and Ghent, R.R., 2008b. Volcanic and impact deposits of the Moon's Aristarchus Plateau: A new view from Earth-based radar images. Geology 36, 135–138, doi:10.1130/G24310A.1.

Campbell, B.A., Putzig, N.E., Carter, L.M., Morgan, G.A., Phillips, R.J., and Plaut, J.J., 2013. Roughness and Near−Surface Density of Mars from SHARAD Radar Echoes. J. Geophys. Res. 118, doi: 10.1002/jgre.20050, 15 p.

Carter, L.M., Campbell, B.A., Holt, J.W., Phillips, R.J., Putzig, N.E., Mattei, S., Seu, R., Okubo, C.H., and Egan, A.F., 2009a. Dielectric properties of lava flows west of Ascraeus Mons, Mars. Geophys. Res. Lett. 36, L23204, doi:10.1029/2009GL041234.

Carter, L.M., Campbell, B.A., Watters, T.R., Phillips, R.J., Putzig, N.E., Safaeinili, A., Plaut, J.J., Okubo, C.H., Egan, A.F., Seu, R., Biccari, D., and Orosei, R., 2009b. Shallow radar (SHARAD) sounding observations of the Medusae Fossae Formation, Mars. Icarus 199, 295–302.

Choudhary, P., Holt, J. W., and Kempf, S. D., 2016. Surface Clutter and Echo Location Analysis for the Interpretation of SHARAD Data From Mars. IEEE Geosci. Remote Sensing Lett., 13, 1285-1289, doi:10.1109/LGRS.2016.2581799.

Fung, A. K., Z. Li, and K. S. Chen, 1992. Backscattering from a randomly rough dielectric surface. IEEE Trans. Geosci. Remote Sens. 30, 356–369, doi:10.1109/36.134085.

Golombek, M.P., R.A. Cook, H.J. Moore, T.J. Parker, 1997. Selection of the Mars Pathfinder landing site. J. Geophys. Res. 102, 3967-3988.

Golombek, M., Redmond, L., Gengl, H., Schwartz, C., Warner, N., Banerdt, B., and Smrekar, S., 2013. Selection of the InSight landing site: Constraints, plans, and progress. Lunar Planet. Sci. XLIV, 1691 (abstract).

Golombek, M., et al. (this issue) Selection of the InSight landing site, Space Sci Rev., submitted.

Grima, C., Kofman,W., Herique, A., Orosei, R., Seu, R., 2012. Quantitative analysis of Mars surface radar reflectivity at 20 MHz. Icarus 220, 84–89, doi:10.1016/j.icarus.2012.04.017.

Grima, C., Schroeder, D. M., Blankenship, D. D. Young, D. A., 2014. Planetary landing-zone reconnaissance using ice-penetrating radar data: Concept validation in Antarctica. Planet. Space Sci. 103, 191–204, doi:10.1016/j.pss.2014.07.018.

Harmon, J.K., Arvidson, R.E., Guinness, E.A., Campbell, B.A., and Slade, M.A., 1999. Mars mapping with delay-Doppler radar. J. Geophys. Res. 104, 14065.

Harmon, J.K., Nolan, M.C., Husmann, D.I., and Campbell, B.A., 2012. Arecibo radar imagery of Mars: The major volcanic provinces. Icarus 220, 990–1030.

Holt, J. W., Peters, M. E., Kempf, S. D., Morse, D. L., and Blankenship, D. D., 2006. Echo source discrimination in single-pass airborne radar sounding data from the Dry Valleys, Antarctica: Implications for orbital sounding of Mars. J. Geophys. Res., 111, E06S24, doi: 10.1029/2005JE002525.

Holt, J.W., Fishbaugh, K.E., Byrne, S., Christian, S., Tanaka, K., Russell, P.S., Herkenhoff, K.E., Safaeinili, A., Putzig, N.E., and Phillips, R.J., 2010. The construction of Chasma Boreale on Mars. Nature 465, 446–449.

Holt, J.W., Safaeinili, A., Plaut, J.J., Head, J.W., Phillips, R.J., Seu, R., Kempf, S.D., Choudhary, P., Young, D.A., and Putzig, N.E., 2008. Radar sounding evidence for buried glaciers in the southern mid-latitudes of Mars. Science 322, 1235–1238.

Kreslavsky, M.A., and Head III, J.W., 2000. Kilometer-scale roughness of Mars: Results from MOLA data analysis. J. Geophys. Res. 105, 26,695–26,711.

Morgan, G.A., Campbell, B.A., Carter, L.M., Plaut, J.J., and Phillips, R.J., 2013. 3D Reconstruction of the Source and Scale of Buried Young Flood Channels on Mars. Science 340, 607–610, doi:10.1126/science.1234787.

Morgan, G. A., B. A. Campbell, L. M. Carter, and J. J. Plaut, 2015. Evidence for the episodic erosion of the Medusae Fossae Formation preserved within the youngest volcanic province on Mars. Geophys. Res. Lett., 42, 7336–7342, doi:10.1002/2015GL065017.

Muhleman, D. O., B. J. Butler, A. W. Grossman, M. A. Slade, 1991. Radar images of Mars. Science, 253, 1508–1513.

Neumann, G.A., Abshire, J.B., Aharonson, O., Garvin, J.B., Sun, X., and Zuber, M.T., 2003. Mars Orbiter Laser Altimeter pulse width measurements and footprint-scale roughness. Geophys. Res. Lett. 30, 1561, doi:10.1029/2003GL017048.

Phillips, R.J., Davis, B.J., Tanaka, K.L., Byrne, S., Mellon, M.T., Putzig, N.E., Haberle, R.M., Kahre, M.A., Campbell, B.A., and Carter, L.M., 2011. Massive CO2 ice deposits sequestered in the South Polar layered deposits of Mars. Science 332, 838.

Phillips, R.J., Zuber, M.T., Smrekar, S.E., Mellon, M.T., Head, J.W., Tanaka, K.L., Putzig, N.E., Milkovich, S.M., Campbell, B.A., Plaut, J.J., Safaeinili, A., Seu, R., Biccari, D., Carter, L.M., Picardi, G., Orosei, R., Mohit, P.S., Heggy, E., Zurek, R.W., Egan, A.F., Giacomoni, E., Russo, F., Cutigni, M., Pettinelli, E., Holt, J.W., Leuschen, C.J., and Marinangeli, L., 2008. Mars north polar deposits: stratigraphy, age, and geodynamical response. Science 320, 1182–1185.

Plaut, J.J., Safaeinili, A., Holt, J.W., Phillips, R.J., Head III, J.W., Seu, R., Putzig, N.E., and Frigeri, A., 2009. Radar evidence for ice in lobate debris aprons in the mid-northern latitudes of Mars. Geophys. Res. Lett. 36, L02203, doi:10.1029/2008GL036379, 4 p.

Putzig, N.E., Phillips, R.J., Campbell, B.A., Holt, J.W., Plaut, J.J., Carter, L.M., Egan, A.F., Bernardini, F., Safaeinili, A., and Seu, R., 2009. Subsurface structure of Planum Boreum from Mars Reconnaissance Orbiter Shallow Radar soundings. Icarus 204, 443–457.

Putzig, N.E., Phillips, R.J., Campbell, B.A., Mellon, M.T., Holt, J.W., Davis, B.J., and Brothers, T.C., 2014. Shallow Radar soundings and surface roughness at past, present, and proposed landing sites on Mars. J. Geophys. Res. 119, 1936–1949, doi:10.1002/2014JE004646.

Shepard, M. K., Campbell, B. A., Bulmer, M. H., Farr, T. G., Gaddis, L. R., Plaut, J. J., 2001. The roughness of natural terrain: A planetary and remote sensing perspective. J. Geophys. Res. 106, pp. 32,777–32,796. doi:10.1029/2000JE001429.

Smith, I. B., and Holt, J. W., 2010. Onset and migration of spiral troughs on Mars revealed by orbital radar. Nature 465, 450-453.

Smith, I. B., Putzig, N. E., Phillips, R. J., and Holt, J. W., 2016. An ice age recorded in the polar deposits of Mars. Science 352, 1075-1078, doi:10.1126/science.aad6968.